Title: A high-sensitive nano-modified biosensor for dynamic monitoring of glutamate and neural spike covariation from rat cortex to hippocampal sub-regions

Authors: Guihua Xiao, Yilin Song, Song Zhang, Lili Yang, Shengwei Xu, Yu Zhang, Huiren Xu, Fei Gao, Ziyue Li, Xinxia Cai

PII: S0165-0270(17)30296-0
DOI: http://dx.doi.org/10.1016/j.jneumeth.2017.08.015
Reference: NSM 7823

To appear in: *Journal of Neuroscience Methods*

Received date: 23-6-2017
Revised date: 11-8-2017
Accepted date: 14-8-2017

Please cite this article as: Xiao Guihua, Song Yilin, Zhang Song, Yang Lili, Xu Shengwei, Zhang Yu, Xu Huiren, Gao Fei, Li Ziyue, Cai Xinxia.A high-sensitive nano-modified biosensor for dynamic monitoring of glutamate and neural spike covariation from rat cortex to hippocampal sub-regions.*Journal of Neuroscience Methods* http://dx.doi.org/10.1016/j.jneumeth.2017.08.015

A high-sensitive nano-modified biosensor for dynamic monitoring of glutamate and neural spike covariation from rat cortex to hippocampal sub-regions

Guihua Xiao[a,b], Yilin Song[a,b], Song Zhang[a,b], Lili Yang[a,b], Shengwei Xu[a,b], Yu Zhang[a,b], Huiren Xu[a,b], Fei Gao[a,b], Ziyue Li[a,b], Xinxia Cai[a,b*]

[a]State Key Laboratory of Transducer Technology, Institute of Electronics, Chinese Academy of Sciences, Beijing 100190, China.

[b]University of Chinese Academy of Sciences, Beijing 10090, China.

[*]Corresponding Email: xxcai@mail.ie.ac.cn;

This work provided a novel nano-modified 16-site implantable microelectrode array (MEA) biosensor used for in vivo dual-mode signals test. In summary, the highlights of the work are:

- The MEA was fabricated with fine structure sharing a similar size with nerve cell.
- The 16 sites were used for glutamate and electrical simultaneously recording.
- The modification was improved. The electrical sites have lower impedence, the Glu sites have higher sensitivity, selectivity and linearity than other works.
- The MEA record dynamic changes of Glu concentration and neural electrical activities in CA1, MoDG, GrDG and CA3 sub-regions.

Abstract

Background: Hippocampus is a critical part of brain tissue involved in many cognitive neural activities. They are controlled by various neurotransmitters such as glutamate (Glu), and affected by electrophysiology.

New method: Herein, we fabricated a 16-site (25μm in diameter) microelectrode array (MEA) biosensor applied in dual-mode tests including Glu and neural spike measurements.

Methods: All the 16 recording sites were electrodeposited with platinum nanoparticles (PtNPs) and 8 sites were used for electrical recording. Glutamate oxidase enzyme (Gluox) and 1,3-Phenylenediamine (mPD) layer were specially modified on the other 8 sites for Glu recording. The dual-mode MEA was implanted from cortex to hippocampus of anesthetized rat to record Glu content and firing rate.

Results: The electrical sites showed much lower impedance. The Glu sites showed much higher sensitivity （7.807 pA/μM）, and ideal selectivity to the major molecules in brain. The post calibration sensitivity (3.935 pA/μM) maintained on a positive level. Different Glu content peaks including cortex (18.32 μM) and hippocampal CA1 (4.39 μM), CA3 (10.16 μM), dentate gyrus (DG, two layers: 5.36 μM and 10.34 μM) have detected. The corresponded firing rate was recorded, too.

Comparison with existing methods: This modification showed much lower impedance and much higher sensitivity. We obtained more neuron activities simultaneously by dual-mode recording. The covariation of Glu and neural spike signals was discovered in the specific hippocampus sub-region.

Conclusions: The covariation between Glu and firing rate changes were synchronous, and effected by regions. The dual-mode signals were useful to find the neurology disease mechanism.

Keywords: hippocampus, glutamate, neural spike, sub-regions, high-sensitive, covariation

1. Introduction

Hippocampus is composed of the hippocampus proper (CA1 and CA3 pyramidal cell layers (Py)) and the dentate gyrus (DG) (D.B.Miller et al., 2005; T.Kadar et al., 1998; Jame G.Greene et al., 2009). As previous studies shown, Alzheimer's disease (AD) probably originated in hippocampal CA1 area, associated with the neurotransmitter concentration and also the abnormal electrical discharge (D.B.Miller et al., 2003). In the hippocampus, the main neurotransmitter is L-Glutamate (Glu) associated with many neuron functions (Riedel et al., 2003). Especially, some specific hippocampal sub-regions possess abundant Glu (Michelle L.Stephens et al., 2011; John Gigg et al., 1994). Normal and abnormal brain functions have relationship with its rapidly self-regulated process, which involved various Glu receptors and correlated transporters (Jorge E.Quintero et al., 2011; Niels C.Danbolt., 2001). Meanwhile, the electrical information was helpful to further

understanding of functional mechanism. However, the limitation of available detection technologies held up our way to get more understandings of specific hippocampus sub-region (Kevin N.Hascup., 2013). In order to overcome this problem encountered in previous studies, electrochemical sensors based on Micro-electromechanical Systems (MEMs) method appeared to record at a sub-second temporal resolution (Jason M.Hinzman et al., 2015).

Presently, many studies were focused on electrochemical, electrophysiological or cell measurements using MEMs technology. Burmeister team has designed ceramic-based multisite microelectrodes for detecting various neurotransmitters (Jason M. Hinzman et al., 2015; Jason J. Burmeister et al., 2008; Jason J. Burmeister et al., 2005). Tina team designed silicon-based four channel microelectrodes to detected dopamine and glutamate (Tina T.-C et al., 2012). Chang team designed nano-channel array platform to transfect cells (Lingqian Chang et al., 2016; Tairong Kuang et al., 2016; Daniel et al., 2016). Chu team and Cai team also designed MEA to measure spontaneous burst firing in rat brain slices (Jun Chu et al., 2012; Yilin Song et al., 2012).

Our group has also worked extensively on Silicon-On-Insulator based microelectrode arrays (MEA) technology that allowed for simultaneously detecting neurotransmitter (Glu) and electrophysiology (neural spike) in vivo. Various coatings were applied on specific electrochemical recording sites to enhance the sensitivity and the selectivity for detecting certain neurotransmitters. And the electrical sites were nano-modified, too. In this paper, we present a novel MEA with electrochemical and electrical recording sites, to directly and accurately measure Glu and neural spike in the hippocampus sub-regions of anesthetized rat. The high sensitive MEA is equipped with high spatial (490 μm^2) and temporal (2 Hz) resolution. Platinum nanoparticles (PtNPs), Glutamate oxidase enzyme (Gluox) and 1,3-Phenylenediamine (mPD) film (PtNPs/Gluox/mPD) were modified on electrochemical sites to selectively measure extracellular Glu. The PtNPs were modified on electrical sites to decrease the impedance.

Glu was firstly converted to hydrogen peroxide (H_2O_2) via Gluox, and H_2O_2 can be oxidized at PtNPs layers when applying optimal voltage by chronoamperometry. Simultaneously, mPD exclusive layer blocked the lager interferents such as ascorbic acid (AA), dopamine (DA), serotonin (5-HT), and 3,4-dihydroxyphenylacetic acid (DOPAC). Compared to our previous work and other studies (Wenjing Wei et al., 2015; Burmeister JJ et al., 2001; Jason J. Burmeister et al., 2002), the sensitivity of electrochemical sites was improved obviously. The MEA biosensor was implanted into the anesthetized rat brain, from cortex to discrete sub-regions of hippocampus. The basal Glu level and electrical signals were monitored simultaneously.

2. Experimental

2.1. Reagents and apparatus

We got Gluox (25U) from Yamasa Corporation (Japan), and bovine serum albumin (BSA, ≥99%) from Amresco (USA). Glutamate sodium(≥99%) and Glutaraldehyde (GA) solution (25% in water) were provided from Shanghai Chemical Reagent Company (China). DA (≥99%) was obtained from Acros Organics (Belgium). DOPAC(≥98%), 5-HT(≥99%) and AA (≥99%) were got from Alfa Aesar Corporation (USA), mPD (≥99%) powder was provided from Aldrich (USA). Urethane (≥98%) powder was purchased from Sinopharm Chemical Reagent company (China).

A BX51 microscope from OLYMPUS was used, the ultrasonic instrument (KH2200E) was obtained from KunShanHeChuang Corporation. The glutamate records were carried out on a potentiostat (Gamry Reference 600, USA). The electrical signals were measured on a 128-channel neuron data recording system

(Blackrock Microsystems, USA). A micropositioner (model 2662, David KOPF instrument, USA) was used to implant MEA probe at a constant speed. We analyzed electrical recording data by Offline Sorter of Plexon Inc in American and NeuroExplorer software of Nex Technologies in American.

2.2. Fabrication of SOI-based MEA

The improved SOI-based MEAs were mass fabricated as our previously described steps (Song Zhang et al., 2016). We designed three photo-masks including recording layer, insulating layer and MEA probe shape layer by L-Edit software. Then, a SOI wafer was used to fabricate the biosensor. Briefly, following cleaning, the photo-mask patterns were transferred onto the wafer in turn using photolithographic procedures. Firstly, the recording layer pattern was transferred onto the clean wafer. This layer consisted of Pt recording sites connected to the bonding pads by Pt connecting lines of approximately 6 mm. Secondly, the insulating layer was transferred onto the recording layer. Si_3N_4 /SiO_2 were used as the insulating layer to insulate the conducting lines against the solution environment. The recording sites and bonding pads was exposed to sensor and transfer the neuron signals. Thirdly, the MEA probe shape layer was used. we need to define an individual MEA biosensor from the silicon substrate that containing 100 MEA biosensors after above two steps. Inductively coupled plasma deep reactive ion etching (ICP DRIE) was used to form the MEA shape.

Four shafts contained 16 recording sites (S1-S16) were close to tips in order to record from deep brain tissue (figure 1(a)). Three Pt rectangular electrodes as auxiliary electrodes were integrated on the MEA for convenience. Each shaft was 85 μm spacing, 100 μm in width, 30 μm in thickness and 6 mm in length. Each tip has four round Pt recording sites (25 μm in diameter) arranged geometrically as a matrix. The distance of two adjacent elements in one sensor matrix was 50 μm such as S9 to S10. The distance of two sites distributed on two shanks was 140 μm to avoid the chemical cross-talk (Pengguang Yu et al., 2000). The left 8 sites (S1-S8) were used as electrical recording sites; the right 8 sites (S9-S16) were used as electrochemical recording sites. In this experiment, all eight electrical sites and one electrochemical site would be used in vivo measurements. The one electrochemical site would work under a suitable voltage. Therefore, chemical cross-talk does not occur in this proposal.

Figure 1

2.3. Modification of MEA

Before modifying procedures, The MEA was cleaned by reactive-ion etching (RIE) for 3 min (vacuum degree$\leqslant$2 Pa; operating air pressure$\leqslant$4.5 Pa; power 40 W; oxygen flow 30 L/min) firstly to ensure the recording sites were absolutely dustless without any contamination or chemicals.

2.3.1 Synthesis of Pt nanoparticles (PtNPs)

All recording sites were firstly modified with Pt nanoparticles (PtNPs). This layer plays a different role in electrochemical and electrical sites. For electrochemical sites, it enlarges the recording surface area and also catalyzes H_2O_2 easily (J.Hu et al., 2010; Jingping Hu et al., 2014). For electrical sites, it decreases the sites' impedance (Song Zhang et al., 2016; Jia Zhang et al., 2010). PtNPs was electro-deposited according to the following procedures. In brief, a three-electrode configuration including Ag/AgCl reference electrode, an integrated Pt auxiliary electrode and MEA working electrode was used in the following all experiments. A 10 mL beaker was used and placed in a recirculating water bath. The synthesis of PtNPs was carried out in a 1:1 mixed solution of 48 mM H_2PtCl_6 and 4.2 mM $Pb(CH_3COO)_2$ at -1.0 V for 30 s. After this procedure, the electrical sites were prepared but not electrochemical sites (figure 1(b)). Figure 1(e) and figure 1(f) show the photograph of PtNPs after modifying with the ordinary microscope and sanning electron microscope (SEM).

2.3.2 Enzyme coatings

Sequentially, the electrochemical sites with PtNPs were coated with Gluox to enzymatic Glu into α-ketoglutarate and H_2O_2. The crosslinking method to immobilize enzyme was used. A 5 μl droplet of enzyme mixture containing 2% Gluox, 1% BSA and 0.125% GA in PBS solution, was left on a waterproof membrane. Then, the right two shafts (S9-S16) were horizontally immersed into the droplet for three times coating under a microscope, 2-3 s stayed inside the droplet and one minute stayed outside to dry would be good for enzyme coating. After modification of Gluox successfully, the MEA must be cured in the room temperature for at least 72 h before their first use.

2.3.3 Electropolymerization of 1,3-Phenylenediamine (mPD)

At last, 1,3-Phenylenediamine (mPD) was electroplated onto the electrochemical sites to restrict interferents from larger molecules and contamination in vivo in order to improve the selectivity. First of all, a standard three-electrode configuration was prepared as described above. The mPD layer was electro-deposited onto S9-S16 by Cyclic Voltammetry (CV) method within the limits of 0 to 0.8 V (scan rate: 100 mV/s; 10 cycles) in the PBS containing 5 mM mPD. Then the MEA tip was removed out, cleaned with DI water and stored for 24 h at room temperature prior to calibration.

Figure 1(c) shows the Glu detecting schematic drawing, PtNPS, Gluox and mPD were coated onto the Glu recording sites surface layer by layer as described. Glu was oxidized into H_2O_2 once contact with Gluox layer on the MEA surface. Then, H_2O_2 diffused through the mPD layer, contacted the PtNPs surface and oxidized at an applied optimal voltage. This reaction frees two electrons per H_2O_2 molecule to flow through our electrochemical detection system and reflected the presence of Glu. The produced signal current was directly proportional to the concentration of Glu.

2.4. In vitro calibration and characterization

In vitro calibration was carried out to generate a standard curve for conversion of Glu current to concentration before in vivo experiment. However, CV was used to get peak oxidation voltage of electrochemical sites. This test was performed in PBS contained 10 mM Glu with limits from -0.4 V to +1.0 V (scan rate: 50 mV/s; 5 cycles). Then, calibrations were carried out in 10 mL fresh continuously-stirred PBS with chronoamperometry. About 20-30 min later, it was suitable time to add the analytes when the baseline was enough stable to sense the changes of concentration. After that, 20 μM, 40 μM, 60 μM, 80 μM, 100 μM Glu and 20 μM AA, DA, 5-HT, DOPAC were added into pure PBS. Eight individual Glu recording sites (S9-S16) were calibrated in this way. The post-calibrations were finished as the pre-calibration procedure above to compare the MEA performance after in vivo experiment.

Meanwhile, impedance was the main factor to influence the neuron-electrical signals. Low impedance would contribute to decrease background current and increase signal to noise ratio. Therefore, the electrical recording sites (S1-S8) were characterized by electrochemical impedance spectroscopy (EIS) method with frequency scanning range from 0.1 Hz to 0.1 MHz under 0.02 V in 10 mL PBS with a three-electrode configuration. The 8 electrical sites were set as working electrode individually.

2.5. In vivo measurements

Sprague–Dawley rats weighing 250-300 g were selected for in vivo experiments. Rat was anesthetized with urethane (20%, 0.7 ml/100 g) and fixed on stereotaxic frame properly. Three craniotomies were needed. The hippocampus site (AP: -3.6 mm, ML: -2.6 mm) for implanting target, the other two sites located on the offside hemisphere (AP: 2 mm, ML: 3.5 mm) for placement of skull nail and (AP: -2 mm, ML: 3.5 mm) for placement of an Ag|AgCl reference electrode that will be fixed on the duramater layer (Matthew D.Johnson

et al., 2008). The MEA was applied to monitor the basal level of Glu from cortex to hippocampus in vivo, and also the corresponding neural spikes changes, especially some key sub-regions in hippocampus such as CA1, DG and CA3. The Glu signal was recorded by Gamry system and the neural spikes was recorded by Blackrock Microsystems. Our MEA was implanted at a constant speed. The depth was recorded all the time by the KOPF micropositioner during implanting. Meanwhile, the simultaneously recorded Glu current and electrophysiology changes were matched with brain depth.

3. Results and discussions

3.1. In vitro calibration and characterization

3.1.1 Cyclic voltammetry (CV) test in Glu solution

CV was used to define the properties of MEA before calibration. Figure 2(a) shows the CV curve of an obvious oxidation peak potential (approximately 0.598 V (~0.6 V)). This potential was considered as the best potential to oxidize Glu and would be used in following calibration and in vivo experiments.

Figure 2

3.1.2 Pre-calibration of Glu sites

The oxidation peak potential of 0.6 V was applied onto the working electrode. The sensitivity and selectivity of MEAs was analyzed. Figure 2(b) shows a typical current-time response curve of one electrochemical site (S9). About 20 min later, the baseline was changeless. The background current was 80±2 pA. Figure 2(c) shows the calibration plot of S9, the sensitivity was 7.807 pA/μM and the linearity was 0.999. However, the average sensitivity (S9-S16) was 6.001±1.194 pA/μM. Figure 2(d) shows the response of additions including 20 μM Glu and interferents. As seen in it, the Glu current responded more than 150 pA, and interferents response are much lower than Glu. Selectivity, the ratio of difference response to Glu response, was all as high as 90%. The average limit of detection (LOD) was 0.56 μM. The calibration results illustrated that all electrochemical sites were reliable to be applied in vivo Glu recording.

Table1 details the performance of our MEA and other previously reported Glu electrodes. The MEA had smaller surface area but higher normalized sensitivity due to the new modification proposal. Compared with other modification, the PtNPs play a significant role in the improvement. On one hand, PtNPs would enhance recording surface area effectively to cross-link much more enzyme because of nanoscale rough surface topography. On the other hand, nanoparticles can catalyze H_2O_2 oxidation at an optimal potential.

Table 1

3.1.3 Post- calibration of Glu sites

The MEA was washed with DI water for three times after in vivo experiments. Figure 2(e) shows post-calibration current-time curve to evaluate the MEA performance. Figure 2(f) shows the calculated sensitivity which decreased to 3.935 pA/μM because of biological contamination. The linearity was 0.996. The selectivity maintained in a stable level of above 90%.

Because of technique limitation, in vivo calibration was extremely difficult to achieve which would be replaced by in vitro calibration. However, studies about pre-calibration and post-calibration were discussed in many researches. Gerhardt team and many other researchers considered that post-calibration was an unreliable method to assess MEA sensitivity because of biological contamination or MEA damage, pre-calibration would be more effective (Gerhardt et al., 2000; Jason J. Burmeister et al., 2002; Wilson GS et

al.,2005). On the contrary, Phillips and Wightman team applied post-calibration results into in vivo experiments (Paul E.M.Phillips et al., 2003; Matthew D.Johnson et al., 2008; Xiomara A.Perez et al., 2009). However, Hinzman team indicated similar results between pre- and post-calibration of Glu MEA (Hinzman JM et al., 2010). However, in our experiment, the pre-calibration was the only possibility in view of the complexity of the sensor array. Considering previous studies and our calibration data, we applied the pre-calibraion (7.807 pA/μM) into in vivo measurements.

3.1.4 Impedance analysis of electrical sites

The electrical sites (S1-S8) were characterized, too. Table.2 details the impedance of the electrical sites at 1 kHz before and after PtNPs modification. Before PtNPs modification, the average impedance of 8 sites was 843.2±79.0 kΩ. After PtNPs modification, the impedance decreased to 13.5±3.8 kΩ, which was significantly reduced to 62.5 times smaller.

Table 2

3.2. In vivo dual-mode measurements

The MEA would cross through the key regions: Py of CA1 (DV:-2250 μm), molecular layer of the dentate gyrus (MoDG, DV:-2840 μm), the granule cells of the dentate gyrus (GrDG, DV:-3020 μm), Py of CA3 (DV：-3400 μm). These sub-regions have abundant glutamaterdic neurons. Figure 3(a) shows structural drawing of hippocampus in the rat brain map. The MEA was implanted from cortex to hippocampus as the MEA path shown. The calibration data were recalled and used to determine the Glu concentration from current changes during in vivo experiments. The electrochemical recording site (S9, sensitivity: 7.807 pA/μM, R=0.999) was selected for neurochemical recording and S1-S8 for electrophysiological recording.

3.2.1 Cortex analysis of dual-mode signals

After preparing all equipment, the MEA was accurately aimed at the center of surgical area (1 mm×1 mm) above hippocampus, and implanted until the MEA tip just arrived at the pia mater. The implanting depth was set as zero. The neural spike and Glu were recorded simultaneously. For Glu recording, it was necessary to get a stable current-time baseline at the pia mater (depth=0). The background current was 106.86±6.36 pA for about 200 s. Then, the MEA was being implanted at 10 μm/s. The Glu current and neural spike connected to the implant depth precisely in order to analyze the covariation.

When the MEA was implanted into the cortex, a large Glu current peak appeared at the depth of 600 μm based on the rat brain stereotaxic map (George Paxinos et al., 2004). The current rose from 106.86 pA to 248.91 pA (equivalently increment of 18.32 μM Glu). On the Glu current curve, we focused on the neural spike release mode of three typical areas including before peak (Point a), on peak (Point b) and after peak (Point c). Each 10 s spike release signals were extracted. Figure 3(c) shows the Glu current peak and the corresponding spike release mode in the cortex. We chose S1-S3 signals from 8 electrical sites. The spikes were single wave regular released (Point a), then changed into the intensive release mode and kept for a while (Point b). The peak value increased from 93 μV to 256 μV. However, the release mode changed into the unregular release style mixing paroxysm and intensive mode with the changes of Glu current (Point c). The peak value kept on about 200 μV. Figure 3(d) shows the firing frequency matched with the Glu current. The peak frequency was 84.67 imp/sec and appeared at the same depth of Glu current peak.

As we know, pyramidal cells existed in the certain area of the cortex. The increase of the Glu current and firing frequency was appeared in the pyramidal cell layer of the cortex. Cortex is the main region to control cerebral function such as movement and sensation. At the regular time, Glu was released from the

cortex and acted on the striatum to balance the DA inhibition action. However, Glu was feedback to the cortex to keep proper function (Mahlon R.Delong et al., 2007). This balance relationship was crucial to avoid Parkinson's disease (PD) caused by disequilibration between excitation and inhibition. From the style of detected spikes release, glutamategic neurons generated an increased current in the cortex. What's more, the sharp MEA tips would stimulate the neurons to be exciting during implanting experiments. Subsequently, the phenomenon of the large Glu current in the cortex was detected many times in many repeated experiments. In the hippocampus, the cortex was a complex tissue to receive signals from other tissue, then integrate and transfer messages to hippocampal sub-region pathways to control our cognition (D.B. Miller et al., 2005).

Figure 3

Glu current decreased slowly with implanting, and some spikes appeared occasionally. Then, the MEA would pass through the corpus callosum (CC). The current decreased to 14.76 pA in CC, and it was considered as baseline level formed by system noise. The following Glu concentration was converted from Glu current subtracted the baseline level firstly.

3.2.2Hippocampus sub-regions analysis of dual-mode signals

Hippocampus was a complex tissue. We focused on the hippocampus sub-regions to investigate the Glu concentration and electrophysiological signals. S9 was used as the Glu site and S1-S8 were used as the electrical sites to record Glu and firing rate simultaneously. When entered into the hippocampus from CC, the MEA was implanted at the speed of 2 μm/s. Figure 4(a) shows four Glu current peaks detected in different hippocampus sub-regions. Figure 3(b) shows the Glu peak concentration. It was 4.39 μM in the CA1, 5.36 μM in the MoDG, 10.34 μM in the GrDG and 10.16 μM in the CA3. Figure 4(b) also shows the firing frequency matched with the Glu current in the hippocampus sub-regions. The values of four firing frequency peaks were 26.33 imp/sec, 42.67 imp/sec, 64.33 imp/sec, 90.67 imp/sec. The Glu current peak and firing frequency peak appeared at the same depth. Meanwhile, the spike release status was extracted. Two electrical sites were chose to analyze the main neural spikes. We combined the dual-mode signals with the implanting depth for sub-regions analysis.

The first Glu current peak appeared at the depth of 2340 μm (Py of CA1). The peak current was about 49.02 pA (equivalent to 4.39 μM Glu). The spike release mode was changed with the current changes. Spike with unregular release mode (Point a) appeared and changed into intensive release mode which mixed with paroxysm release style (Point b). Then, the spike released with unregular release mode later (Point c).

With the implantation process, the electrical signals and the Glu current was detected all the time. The second Glu current peak appreared at the depth of 2880 μm (MoDG). The peak current was about 58.39 pA (equivalent to 5.36 μM Glu). The spike released with intensive release mode (Point d). The frequency was higher than before and the amplitudes were as high as 248 μV. For a moment, the current decreased to 17.26 pA rapidly and the spike frequency became lower (Point e).

The third Glu current peak appeared at the depth of 3180 μm (GrDG). The peak current was about 97.94 pA that was equivalent to 10.34 μM Glu. The spike was intensively released with increasing frequency (Point f). As the current decreased, the spike frequency decreased and changed into the unregular release mode (Point g). The GrDG layer consists of roundlet or oval cells with dense arrangement. Its neuraxon called mossy fibers connected with neuron-dendrite of pyramidal cell. This synapse contains Glu and has ability to release Glu. GrDG is considered as the main sub-region of abundant Glu.

When the MEA was advanced to the next sub-region, the current peak appeared at the depth of 3420 μm (Py layer of CA3). A current peak of 97.58 pA (equivalent to 10.16 μM Glu) was detected. The spikes with large amplitude were intensive released (Point h).

Hippocampus is the key region to control memory, learning and cognition. However, Glu was the chief neurotransmitter in hippocampus that mainly released in DG, CA1 and CA3. The pyramidal cell layer and molecular layer release amounts of Glu than other layers because of glutamatergic system. Many studies focused on hippocampus especially the sub-regions of CA1, CA3 and DG. Most of researchers focused on Glu release or hippocampus firing characters (Michelle L.Stephens et al., 2011; Guoqiang Bi et al., 1998). However, the covariation of dual mode signals has not been mass detected. Some related researches indicate that the neuron will keep firing but the neurotransmitter would not change during frequency-dependent stimulation (Matthew D. Johnson et al., 2008; G.C. Albert et al., 2009; R. Mark Wightman et al., 1990; Carrie E. John et al., 2006). From our results, the Glu current and the firing frequency was changed similarly at the same region. The Glu current increase in the special regions and the firing frequency increase, too. They all appeared at the layer possessed abundant pyramidal cells. The covariation between Glu and firing rate was obvious and related with the brain region.

Figure 4

Taken all continuous recording electrical signals for consideration, Figure 5 shows various patterns of spike extracted from the cortex, CA1, DG and CA3. Different patterns were showed with different colors. In the cortex, spike amplitude from 78 μV to 280 μV has all detected. The amplitude increased during implanting deeply and come to largest at the four layer of the cortex which has numerous pyramidal neurons. In the hippocampus sub-regions, a typical inverse spike appeared successively. The amplitude was from 130 μV to 295 μV. As figure 5 shown, the spike detected by S1 in the cortex was a typical pyramidal neuron with character of thin and tall peak. Many other studies showed CA1 was formed with small pyramidal cells and CA3 was mainly big pyramidal cells (T.Kadar et al., 1998). This spikes showed CA3 sub-region has bigger amplitude because of neuron styles. The detected discharge styles have their own characters. The un-regulated released spikes always along with paroxysm and intensive release modes. The spikes with single wave regular release style have the biggest peak-to-peak value and often following intensive released spikes with high frequency. This intensive release mode showed with decreasing amplitude until disappeared. In all 8 electrical recording sites, different sites have detected different release styles at one sub-region.

Figure 5

4. Conclusion

The MEA biosensor was modified with a novel proposal to record Glu and neural spike simultaneously. The two signals covariation was analyzed too. For chemical sites, the sensitivity and selectivity was much higher than previous studies. For electrical sites, impedance has decreased 62.5 times in 1 kHz. The MEA was used to detect basal Glu level and neural spike from cortex to hippocampus. Different Glu concentration and firing frequency in sub-region CA1, DG and CA3 were monitored. From the matched dual-mode signals covariation, the spike release mode and firing frequency was changed with Glu current. The release frequency of spikes was low and mainly with the single wave regular release when the current was stable. However, with the increase of current, the frequency was higher than before with intensive release. Then, frequency and amplitude became low with the current decreasing. Moreover, different spike patterns were discovered in cortex and hippocampus. In the hippocampus, typical big centrum cell was detected. Those

spikes were thinner and taller than the spikes in cortex. Our designed MEA was successfully used in the vitro and in vivo experiment. We would focus on the disease models to discover more pathogenic factors by dual-mode measurement.

Acknowledgements

This work was sponsored by the National Key Research and Development Program of China (2017YFA0205900), the NSFC (No.61527815, No.61501426, No.31500800, No.61601435), the Beijing Science and Technology Plan (Z141100000214002, Z161100004916001), National Science and Technology Major Project (2014CB744600), and the Key Research Programs (KJZD-EW -L11-2, QYZDJ-SSW-SYS015) of Frontier Sciences,CAS.

Conflicts of Interest

The authors declare no conflict of interest.

Reference

Burmeister JJ, Gerhardt G, 2001. Self-referencing ceramic-based multisite microelectrodes for the detection and elimination of interferences from the measurement of L-glutamate and other analytes. Anal Chem.73,1037–1042.

Carrie E. John, Evgeny A. Budygin, Yolanda Mateo, Sara R. Jone, 2006. Neurochemical characterization of the release and uptake of dopamine in ventral tegmental area and serotonin in substantia nigra of the mouse. Journal of Neurochemistry. 96, 267-282.

D.B. Miller and J.P. O'Callaghan, 2003. Effects of Aging and Stress on Hippocampal Structure and Function. Metabolism. 52(10), 17-21.

D.B. Miller, J.P. O'Callaghan, 2005. Aging, stress and the hippocampus. Ageing Research Reviews.4, 123-140.

Daniel Gallego-Perez et al, 2016, On-Chip Clonal Analysis of Glioma-Stem-Cell Motility and Therapy Resistance. Nano letters. 16, 5326-5332.

G.C. Albert, C.M. Cook, F.S. Prato, A.W. Thomas, 2009. Deep brain stimulation, vagal nerve stimulation and transcranial stimulation: An overview of stimulation parameters and neurotransmitter release. Neuroscience and Biobehavioral Reviews. 33, 1042–1060.

George Paxinos,Charles Watson,2004. The rat brain in stereotaxic coordinates.pp.103-106.

Guoqiang Bi, Muming Poo, 1998. Synaptic modifications in cultured hippocampal neurons:Dependence on spike timing, synaptic strength, and postsynaptic cell type. The Journal of Neuroscience. 18(24), 10464–10472.

Hinzman JM, Thomas TC, Burmeister JJ et al, 2010. Diffuse brain injury elevates tonic glutamate levels and potassium-evoked glutamate release in discrete brain regions at two days post-injury:an enzyme-based microelectrode array study. J Neurotrauma.27, 889-899.

Jorge E. Quintero, François Pomerleau, Peter Huettl, Kirk W. Johnson,James Offord, Greg A. Gerhardt,2011. Methodology for rapid measures of glutamate release in rat brain slices using ceramic-based microelectrode arrays:Basic characterization and drug pharmacology. Brain Research. 1402,1-9.

James G.Greene,Karin Borges, Raymond Dingledine,2009. Quantitative transcriptional neuroanatomy of the rat hippocampus: evidence for wide-ranging, pathway-specific heterogeneity among three principal cell layers. Hippocampus. 19(3), 253-264.

John Gigg, Aiko M. Tan, and David M. Finch, 1994. Glutamatergic Hippocampal Formation Projections to Prefrontal Cortex in the Rat Are Regulated by GABAergic Inhibition and Show Convergence With Glutamatergic Projections From the Limbic Thalamus. Hippocampus. 4(2), 189-198.

Jason J. Burmeister, Francois Pomerleau, Michael Palmer, Brian K. Day, Peter Huettl, Greg A. Gerhardt, 2002. Improved ceramic-based multisite microelectrode for rapid measurements of L-glutamate in the CNS. 119, 163-171.

Jason J. Burmeister, Francois Pomerleau, Peter Huettl, Clelland R. Gash,Catherine E. Werner, John P. Bruno, Greg A. Gerhardt, 2008. Ceramic-based multisite microelectrode arrays for simultaneous measures of choline and acetylcholine in CNS. Biosensors and Bioelectronics. 23, 1382–1389.

Jason J. Burmeister, Michael Palmer, Greg A. Gerhardt, 2005 l-lactate measures in brain tissue with ceramic-based multisite microelectrodes. Biosensors and Bioelectronics. 20, 1772–1779.

Jason M. Hinzman,n, Justin L. Gibson, Ryan D. Tackla, Mark S. Costello,Jason J. Burmeister, Jorge E. Quintero, Greg A. Gerhardt, Jed A. Hartings,2015. Real-time monitoring of extracellular adenosine using enzyme-linked microelectrode arrays. Biosensors and Bioelectronics.74,512-517.

J. Hu, X. Lu, J.S. Foord,2010. Nanodiamond pretreatment for the modification of diamond electrodes by platinum nanoparticles. Electrochemistry Communications. 12,676-679.

Jingping Hu, Sirikarn Wisetsuwannaphum and John S. Foord,2014. Glutamate biosensors based on diamond and graphene platforms. Faraday Discussions.172,475-472.

Jia Zhang,Jing Li,Fan Yang,Bailin Zhang,Xiurong Yang,2010. Pt nanoparticles-assisted electroless depositon of Prussian blue on the electrode: Detection of H_2O_2 with tunable sensitivity.Journal of Electroanalytical Chemistry.638,173-177.

Jun-Uk Chu, Mee Jee Jeong, Kang-Il Song, Heui-Chang Lee, Jinseok Kim, Yong-Jun Kim,Kuiwon Choi, Jun-Kyo Francis Suh, Inchan Youn, 2012. spontaneous synchronized burst firing of subthalamic nucleus neurons in rat brain slices measured on multi-electrode arrays.Neuroscience Research. 72, 324–340 .

Kevin N.Hascup,Erin R.Hascup,Greg A.gerhardt et al,2013.Microelectrode array fabrication and optimization for selective neurochemical detection.Neuromethods. 80,27-29.

Lingqian Chang et al 2016 Controllable Large-Scale Transfection of Primary Mammalian Cardiomyocytes on a Nanochannel Array. Small, 12(43), 5971-5980

Michelle L.Stephens, Jorge E.Quintero, Francois Pomerleau, Peter Huettl, and Greg A.Gerhardt, 2011. Age-related changes in glutamate release in the CA3 and dentate gyrus of the rat hippocampus. Neurobiol Aging. 32(5), 811-820.

Mahlon R.Delong, Thomas Wichmann,2007.Circuits and circuit disorders of the basal ganglia.Neurologigal review.64,20-23.

Matthew D.Johnson,Robert K.Franklin, Daryl R.Kipke, et al,2008. Implantable microelectrode arrays for simultaneous electrophysiological and neurochemical recordings. Journal of Neuroscience methods.174,62-70.

Niels C.Danbolt, 2001. Glutamate uptake.Progress in Neurobiology.65,1-21.

Paul E.M.Phillips, R.Mark Wightman,2003. Critical guidelines for validation of the selectivity of in-vivo chemical microsensors. Trends in Analytical Chemistry. 22(9),509-514.

Pengguang Yu and George S.Wilson, 2000. An independently addressable microbiosensor array:What are the limit of sensing element density? Faraday Discuss. 116, 305-317

Riedel G, Platt B, Micheau J, 2003. Glutamate receptor function in learning and memory. Brain Research. 140,1–47.

R. Mark Wightman, Jayne B. Zimmerman, 1990. control of dopamine extracellular concentration in rat striatum by impulse flow and uptake. Brain Research Reviews. 15, 135-144.

Song Zhang, Yilin Song, Mixia Wang, Zhiming Zhang, Xinyi Fan,Xianteng Song, Ping Zhuang, Feng Yue, Piu Chan, Xinxia Cai,2016. A silicon based implantable microelectrode array for electrophysiological and dopamine recording from cortex to striatum in the non-human primate brain.Biosensors and Bioelectronics 85,53-61.

T.Kadar, S.Dachir, B.Shukitt-Hale, A.Levy, 1998. Sub-regional hippocampal vulnerability in various animal models leading to cognitive dysfunction. J Neural Transm.105, 987-1004.

Tina T.-C. Tseng, Harold G. Monbouquette, 2012. Implantable microprobe with arrayed microsensors for combined amperometric monitoring of the neurotransmitters , Glutamate and Dopamine. Journal of Electroanalytical Chemistry. 682, 141–146.

Tairong Kuang, Lingqian Chang, Xiangfang Peng, Xianglong Hu, Daniel Gallego-Perez, 2016. Molecular beacon nano-sensors for probing living cancer cells. Trends in Biotechnology. 35, 4 1-13

Wassum K M,Tolosa V M,Wang et al,2008. Silicon wafer-based platinum microelectrode array biosensor for near real-time measurement of glutamate in vivo. Sensor.8(8),5023-5036.

Wenjing Wei, Yilin Song, Li Wang, Song Zhang, Jinping Luo, Shengwei Xu , Xinxia Cai,2015. An implantable microelectrode array for simultaneous L-glutamate and electrophysiological recordings in vivo.Microsystem&Nanoengineering.1, 1-6.

Wilson GS, Gifford R,2005.Biosensors for real-time in vivo measurements. Biosens Bioelectron.20,2388-2403.

Xiomara A.Perez, Kathryn T.O'Leary, Maryka Quik et al. 2009.Prominent role of a3/a6b2* nAChRs in regulating evoked dopamine release in prime putamen: effect of long-term nicotine treatment. Molecular Pharmacology 75(4):938.

Yibai Hu, Kim M.Mitchell, Fakhrildeen N.Albahadily, Elias K.Michaelis, George S.Wilson, 1994. Direct measurement of glutamate release in the brain using a dual enzyme-based electrochemical sensor. Brain Research 659(1-2),117-125.

Yilin Song, Nansen Lin, Chunxiu Liu, Hong Jiang, Guogang Xing, Xinxia Cai 2012. A novel dual mode microelectrode array for neuroelectrical and neurochemical recording in vitro. Biosensors and Bioelectronics 38 416–420.

Figure Captions

Figure.1 Structure of MEA with different modification layers including electrical sites and Glu sites. (a) Layout of the improved SOI-based MEA with four shafts and 16 sites. Each shaft was 85 μm spacing, 100 μm in width, 30 μm in thickness and 6 mm in length. The center to center distance distributed on two shanks was 140 μm. The distance between the sensor matrix elements was 50μm such as S13 to S16. The left 8 sites (S1-S8) were used as electrical recording sites; the right 8 sites (S9-S16) were used as electrochemical recording sites. (b) The electrical recording sites (S1-S8) with PtNPs modification. (c) The Glu recording sites (S9-S16) with three different layers (PtNPs/Gluox/mPD). The right schematic drawing shows function of various layers for detection of Glu on the MEA. (e) The 16 sites show black because of Pt nanoparticles modification under the microscope. The specific sites number was showed in red. (f) The photograph of Pt nanoparticles on the site display nano partical size by sanning electron microscope (SEM, 30K).

Figure 2. Pre ((a)-(d)) and post ((e)-(f)) calibrations of Glu sites. (a) CV of S9 in the PBS with 10 mM Glu. (b) A typical pre calibration Current-Time curve of S9. 20 μM, 40 μM, 60 μM, 80 μM, 100 μM Glu and 20μM AA, DA, 5-HT and DOPAC were added into the pure solution in turn. (c) The Glu Current-Concentration response curve of pre calibration. (d) Current responses of additions including 20 μM Glu, AA, DA, 5-HT and DOPAC. (e) A typical post calibration Current-Time response curve of S9. 20 μM AA, DA, 5-HT, DOPAC and 20 μM, 40 μM, 60 μM, 80 μM Glu were added into the PBS. (f) The post calibration curve of sensitivity (3.935 pA/μM) and maintained linearity (R=0.996).

Figure 3. The brain map and covariation of Glu and firing properties in cortex. (a) The rat hippocampus structural drawing. The MEA was implanted from cortex to hippocampus. (b) Comparison of the detected Glu current peaks in the cortex and hippocampus sub-regions. (c) Glu current peak in the cortex. Three typical areas (Point a, Point b, Point c) was analyzed by matching with neural spike release mode. (d) The firing frequency matched with the Glu current changes during implanting. They changed with the similar trend.

Figure 4. Connection between Glu current changes and the responding spikes in hippocampus sub-regions. (a) Four peaks detected in sub-regions of hippocampus including CA1, MoDG, GrDG and CA3. Each peak matched with the corresponding spikes release mode of 10 s in many key areas. (b) The firing frequency matched with the Glu current changes in the hippocampus sub-regions. The two parameters changed with the similar trend.

Figure 5. Different patterns were detected from cortex to hippocampus sub-regions in 8 electrical sites. Different patterns were showed with different colors which distributed in cortex, CA1, DG and CA3.

Table 1 Comparison of other interrelated electrochemical sensors.

Table 2 The electrical sites (S1-S8) impedance by EIS (1 kHz).

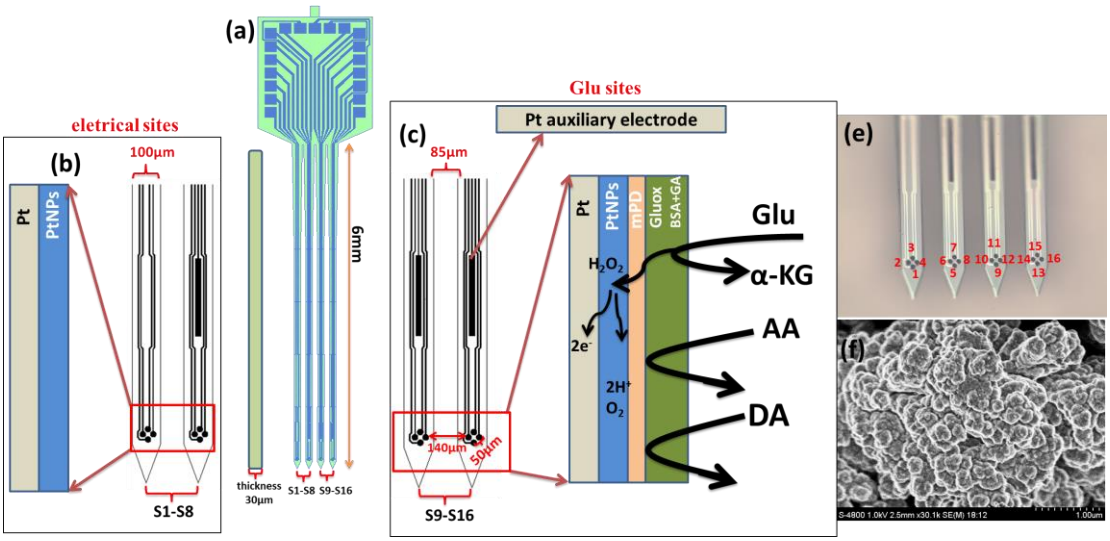

Figure.1 Structure of MEA with different modification layers including electrical sites and Glu sites. (a) Layout of the improved SOI-based MEA with four shafts and 16 sites. Each shaft was 85 μm spacing, 100 μm in width, 30 μm in thickness and 6 mm in length. The center to center distance distributed on two shanks was 140 μm. The distance between the sensor matrix elements was 50μm such as S13 to S16. The left 8 sites (S1-S8) were used as electrical recording sites; the right 8 sites (S9-S16) were used as electrochemical recording sites. (b) The electrical recording sites (S1-S8) with PtNPs modification. (c) The Glu recording sites (S9-S16) with three different layers (PtNPs/Gluox/mPD). The right schematic drawing shows function of various layers for detection of Glu on the MEA. (e) The 16 sites show black because of Pt nanoparticles modification under the microscope. The specific sites number was showed in red. (f) The photograph of Pt nanoparticles on the site display nano partical size by sanning electron microscope (SEM, 30K).

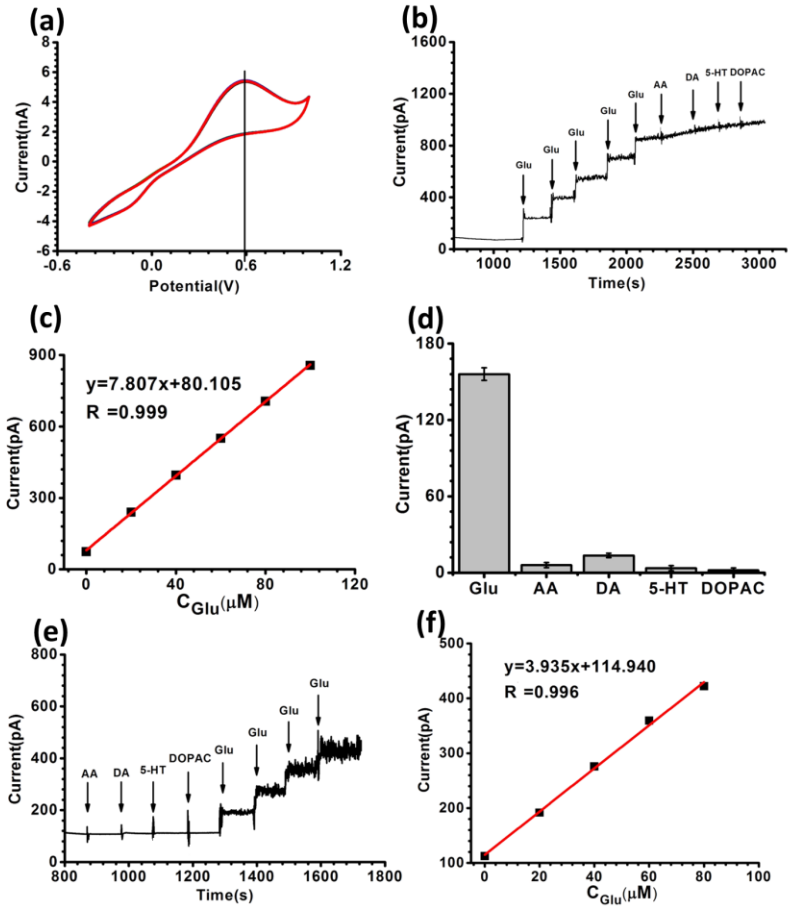

Figure 2. Pre ((a)-(d)) and post ((e)-(f)) calibrations of Glu sites. (a) CV of S9 in the PBS with 10 mM Glu. (b) A typical pre calibration Current-Time curve of S9. 20 μM, 40 μM, 60 μM, 80 μM, 100 μM Glu and 20μM AA, DA, 5-HT and DOPAC were added into the pure solution in turn. (c) The Glu Current-Concentration response curve of pre calibration. (d) Current responses of additions including 20 μM Glu, AA, DA, 5-HT and DOPAC. (e) A typical post calibration Current-Time response curve of S9. 20 μM AA, DA, 5-HT, DOPAC and 20 μM, 40 μM, 60 μM, 80 μM Glu were added into the PBS. (f) The post calibration curve of sensitivity (3.935 pA/μM) and maintained linearity (R=0.996).

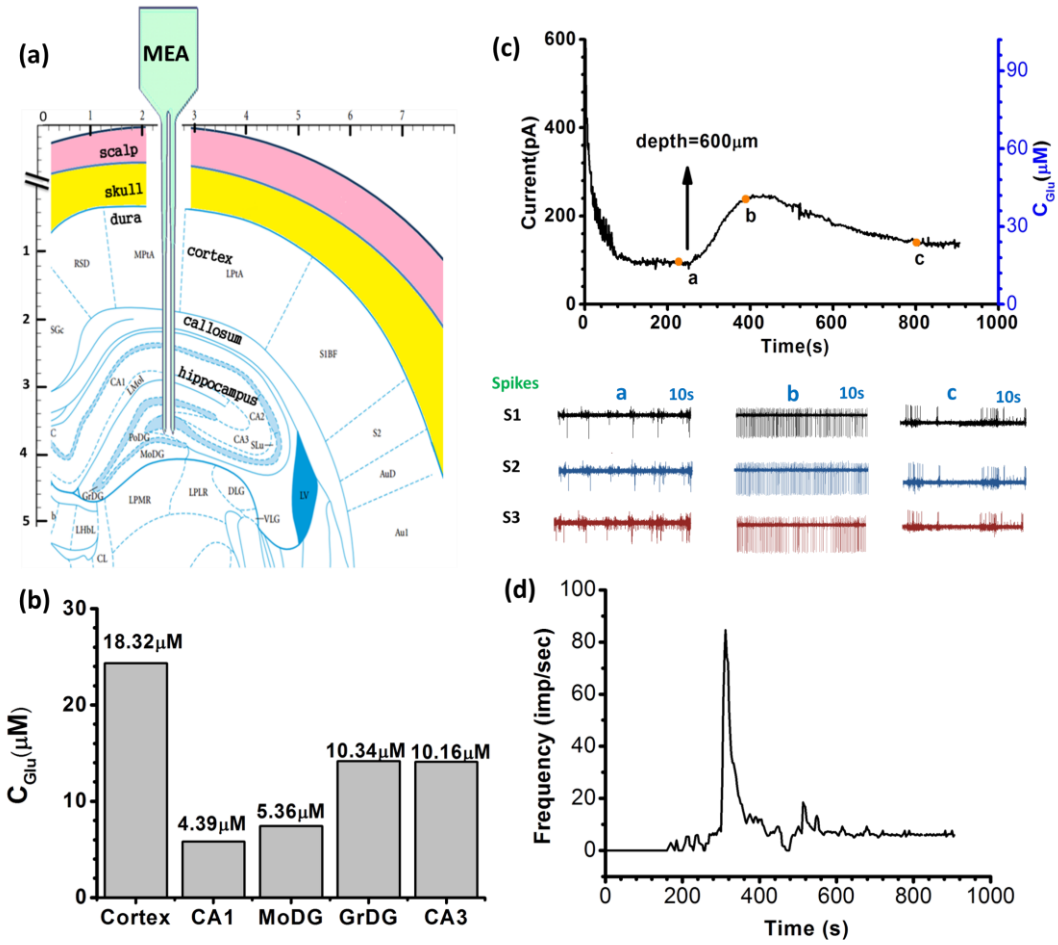

Figure 3. The brain map and covariation of Glu and firing properties in cortex. (a) The rat hippocampus structural drawing. The MEA was implanted from cortex to hippocampus. (b) Comparison of the detected Glu current peaks in the cortex and hippocampus sub-regions. (c) Glu current peak in the cortex. Three typical areas (Point a, Point b, Point c) was analyzed by matching with neural spike release mode. (d) The firing frequency matched with the Glu current changes during implanting. They changed with the similar trend.

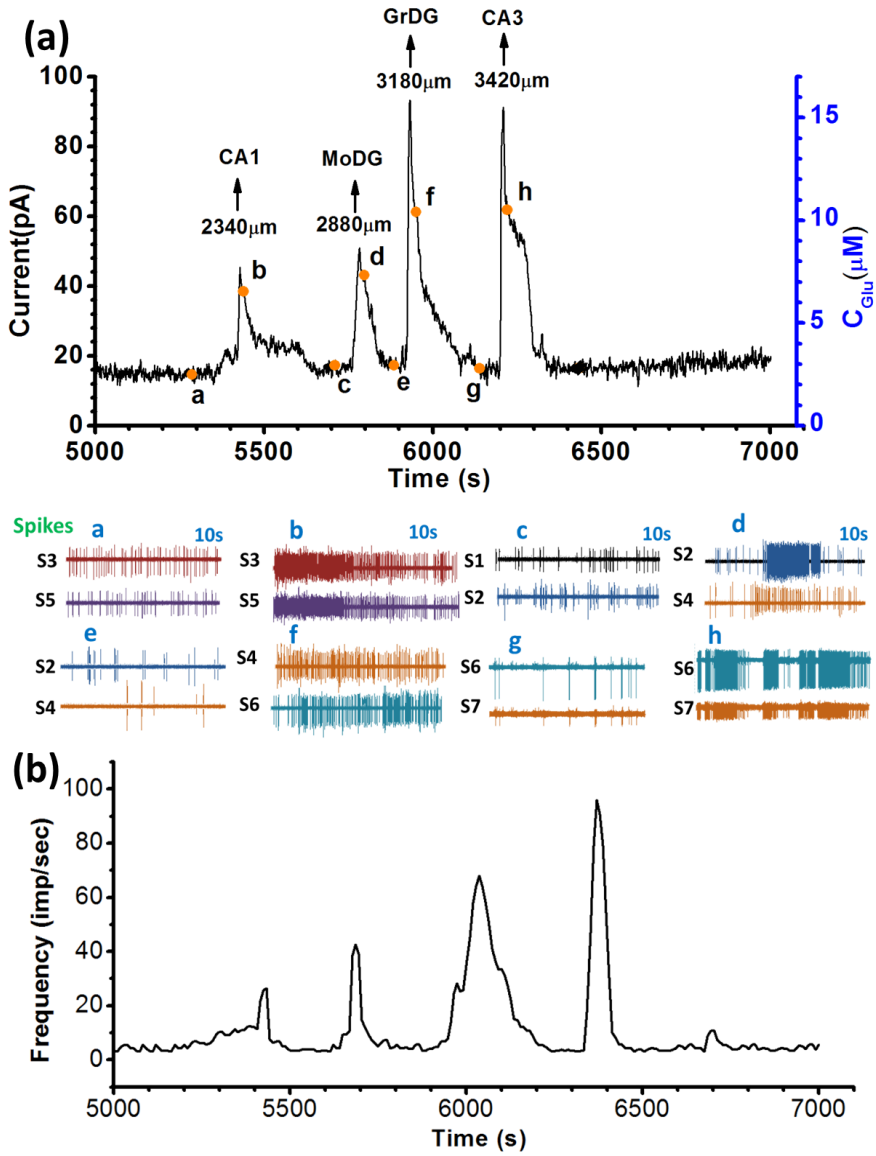

Figure 4. Connection between Glu current changes and the responding spikes in hippocampus sub-regions. (a) Four peaks detected in sub-regions of hippocampus including CA1, MoDG, GrDG and CA3. Each peak matched with the corresponding spikes release mode of 10 s in many key areas. (b) The firing frequency matched with the Glu current changes in the hippocampus sub-regions. The two parameters changed with the similar trend.

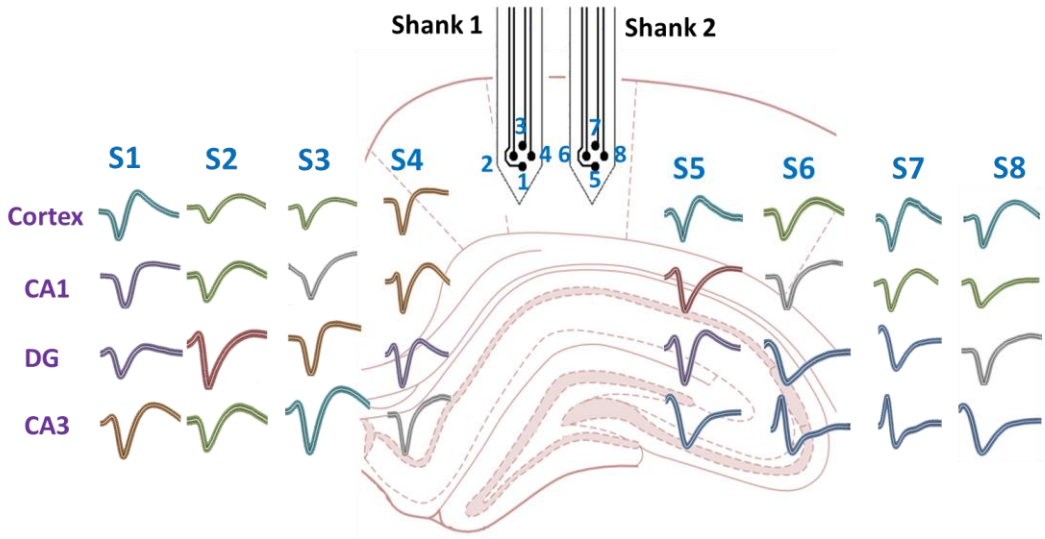

Figure 5. Different patterns were detected from cortex to hippocampus sub-regions in 8 electrical sites. Different patterns were showed with different colors which distributed in cortex, CA1, DG and CA3.

Table 1 Comparison of other interrelated electrochemical sensors.

Modify	**Area (μm^2)**	**Sensitivity (pA/ μM/ μm^2)**	**LOD (μM)**	**Test Interferent**	**Reference**
Pt /Gluox/Nafion	5.49×10^{5}	2.37×10^{-4}	0.2	AA,DA, NE, 5-HT, DOPAC	Yibai Hu,et al,1994
Pt/Gluox/Nafion	7500	2.23×10^{-3}	0.5	Anion species	Burmeister,et al,2001
Pt/Gluox/mPD	4995	6.81×10^{-4}	0.8	AA,DA,5-HT,DOPAC	Jason M Hinzman,et al,2010
Ppy/Nafion/Gluox	4800	5.17×10^{-4}	0.79	AA,DA	Wassum KM,et al,2008
Pt/PtNPs/Gluox/mPD	490	1.22×10^{-2}	0.56	AA,DA,5-HT,DOPAC	This paper

Table 2 The electrical sites (S1-S8) impedance by EIS (1 kHz).

Sites	S1	S2	S3	S4	S5	S6	S7	S8	Average
Pre (kΩ)	777.8	759.5	812.3	992.2	935.2	817.6	879.0	771.7	843.2±79.0
Post (kΩ)	16.4	14.7	16.94	14.9	16.64	14.1	7.3	7.0	13.5±3.8